ESRF	**Experiment title:** Exploring biaxial nematic order in graphene oxide nanocomposites	**Experiment number**: MA-4888
Beamline: ID02	**Date of experiment**: from: 15 July 2021 to: 18 July 2021	**Date of report**: 12 September 2022
Shifts: 9	**Local contact(s)**: Peter Boesecke	*Received at ESRF:*

Names and affiliations of applicants (* indicates experimentalists):

Prof. Francesco Vita *, Prof. Oriano Francescangeli *, Dr. Luigi Montalto *, Dip. SIMAU, Università Politecnica delle Marche, via Brecce Bianche, I-60131, Ancona, Italy

Report:

The experiment aimed to study the structural properties of a novel nanocomposite system obtained by mixing two liquid crystalline aqueous solutions: the lyotropic nematic (N) phase formed by poly(2,2'-disulfonyl-4,4'-benzidine terepthalamide) (PBDT), a rod-like aramid polyelectrolyte, and the colloidal N phase comprised of graphene oxide (GO) platelets. Our interest in the resulting hybrid (PBDT + GO) liquid crystal solution derived from the possibility to use it to cast nanocomposite films with exceptional mechanical properties.

During the experiments we measured three series of samples:

- acqueous GO solutions at different concentrations for three different flake sizes (36 samples);
- neat PBDT solutions in water at different concentration (15 samples);
- hybrid PBDT + GO solutions in water at different combinations of PBDT and GO concentrations (35 samples).

Simultaneous SAXS and WAXS measurements were performed on all the samples, with the former carried out at three different sample to detector distances (SDD = 1 m, 10 m and 30 m) in order to cover an extended q-range. An Eiger2 4M photon counting detector and a Ryonix LX 170HS CCD detector were used for SAXS and WAXS measurements, respectively. Because of the high viscosity of many samples, we could not use the flow-through cell available on ID02 and measurements were performed in glass capillaries. Unfortunately, this resulted in a suboptimal background subtraction, as the optical path was sligthly different for each sample. In spite of this limitation, the acquired data still provided a large amount of structural information on the investigated samples.

A few unsuccesfull attempts were made to align the samples by placing them under a static magnetic field for a few hours. In addition, lack of time prevented us from performing measurements on samples sandwiched between thin planar surfaces.

The detailed analysis of the experimental data is still ongoing. Below we summarize some of the results obtained so far.

GO solutions.

A few representative examples of 2D SAXS patterns taken on GO solutions (flake diameter ~1-2 μm) are shown in Fig. 1 for different concentrations (SDD = 10 m). For a concentrations higher than 0.3 wt%, the scattering was clearly anisotropic, indicating the formation of a nematic phase, with the GO platelet normal aligned hortogonally to the capillary axis (vertical in all figures). At lower concentrations, the patterns became isotropic,

indicating the loss of nematic order. For anisotropic patterns, fitting the azimuthal intensity profile allowed us to estimate the nematic order parameter S, obtaining values close to $S = 0.65$.

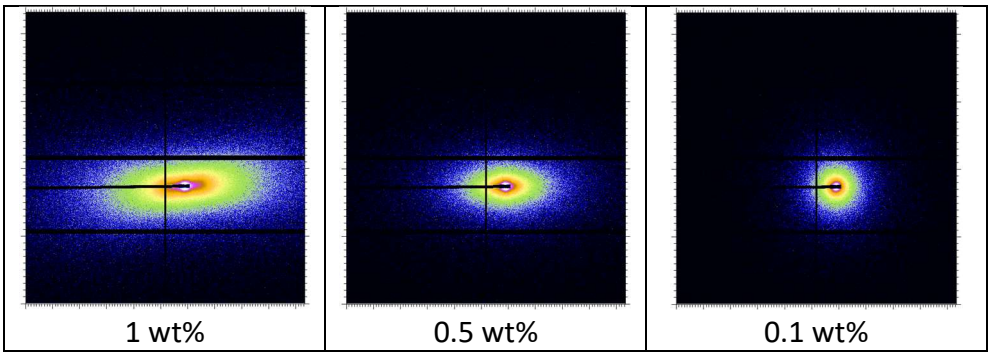

Figure 1.

Fig. 2 shows the SAXS radial intensity profiles, measured along the main scattering direction for anisotropic patterns or azimuthally averaged for isotropic patterns. The extended q range is obtained by merging the profiles from the patterns taken at three different detector distances. Looking at the curves of the high concentration samples (2-0.3 wt%), one can observe:

- a decrease of the scattered intensity with a q^{-2} power law;
- the presence of a broad peak shifting towards lower q values with decreasing concentration.

The former behavior is a typical signature of scattering from flat 2D particles; the latter represents a weak interference factor, i.e. the presence of a short-range positional correlation among GO platelets, and will be discussed in the following. The q^{-2} power law is preserved down to the lowest q-values, indicating that the particles are flat up to a length scale of the order of 600 nm.

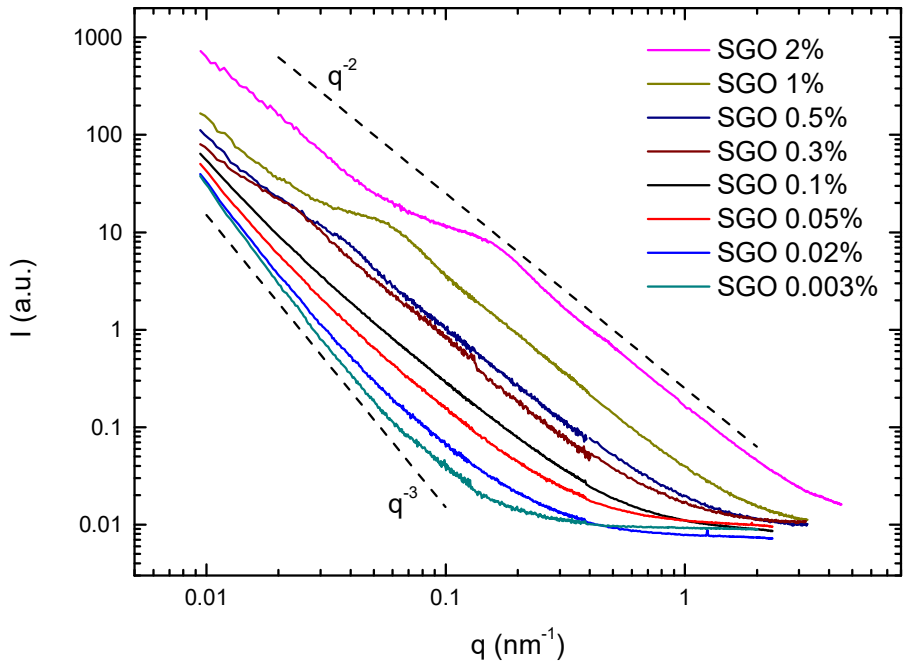

Figure 2

By contrast, the behavior of low concentration samples is significantly different, as:

- no peak is visible;
- the slope of the curve becomes more negative, approaching a q^{-3} power law.

Looking at low concentration curves more in detail it can be noticed the presence of two regions: a larger q region, where the curves can still be fitted by a q^{-2} power law, and a lower q region, where the behavior follows a q^{-n} power law with n changing from 2.5 (at 0.1% concentration) to 3.2 (at 0.003% concentration). A value of n larger than 2 is typically associated to a fractal structure of the scatterer (self-similar roughness), thus suggesting the wrinkling of the platelets (see Weir et al., Chem, Mater. 2016, 28, 1698). The lower limit of the q^{-2} region shifts towords larger q values as the concentration decreases, suggesting a progressive reduction of the particle flatness, down to a lateral size of about the order of 100 nm, as the concentration decreases. It seems reasonable that, at high concentrations, the stronger interaction between adjacent platelets promotes a flatter geometry and a more ordered stacking.

As mentioned above, a weak broad peak is visible in the spectra of the high concentration samples, indicating the presence of some positional order among the platelets. This peak is more evident if one looks at the structure factor, i.e. if one divides the scattered intensity $I(q)$ by the particle form factor ($\propto q^{-2}$) as in Fig. 3.

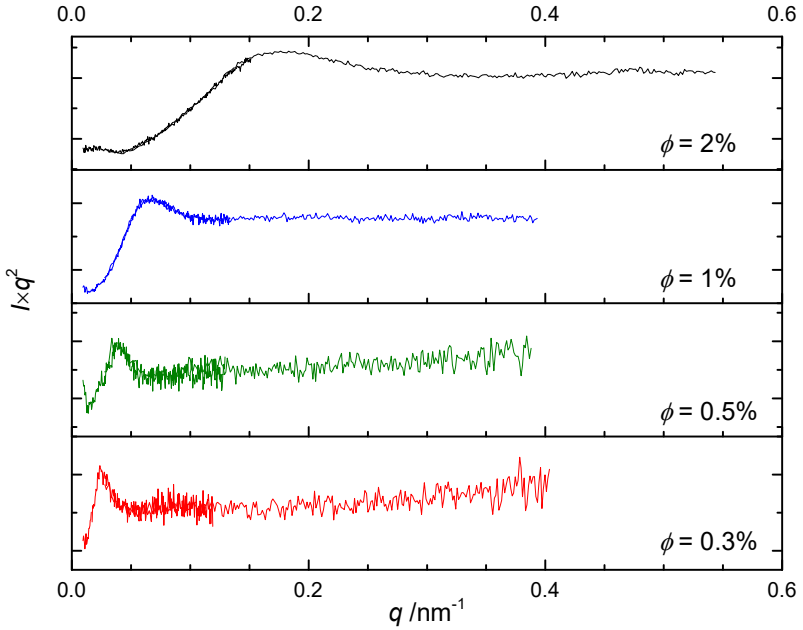

Figure 3.

The peak position clearly shifts toward lower q values as the concentration decreases. This corresponds to an inter-particle spacing d changing from 35.8 nm at a concentration of 2 wt% to 247 nm at 0.3 wt% (Fig. 4). For lamellar systems, the 1D swelling model predicts a d spacing inversely proportional to the volume fraction ϕ, with the proportionality constant being equal to the lamellar thickness t: $d = t/\phi$. Our data agree quite well with this model (inset of Fig. 4), providing a lamellar thickness t = (0.51 ± 0.02) nm, in agreement with other GO data reported in the literature.

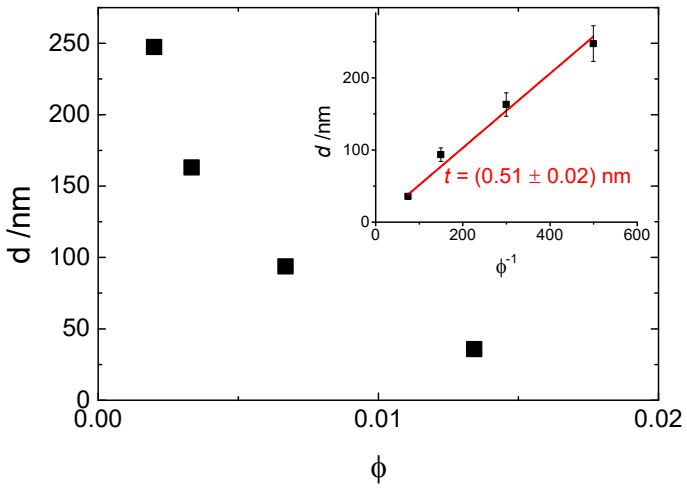

Figure 4.

Neat PBDT and PBDT-GO solutions.

A few representative SAXS diffraction patterns (SDD = 1 m) are shown in Fig. 5 for neat PBDT solutions at different concentrations: at large concentrations the pattern is clearly anisotropic, with a pair of diffraction spots aligned along the equatorial direction suggesting nematic order with the polymer rod aligned along the capillary axis. For intermediate concentrations, between 1 and 0.3 wt%, the diffraction spots change into an isotropic diffraction ring, indicating the loss of nematic order. Finally, below 0.3 wt%, no diffraction spot was observed.

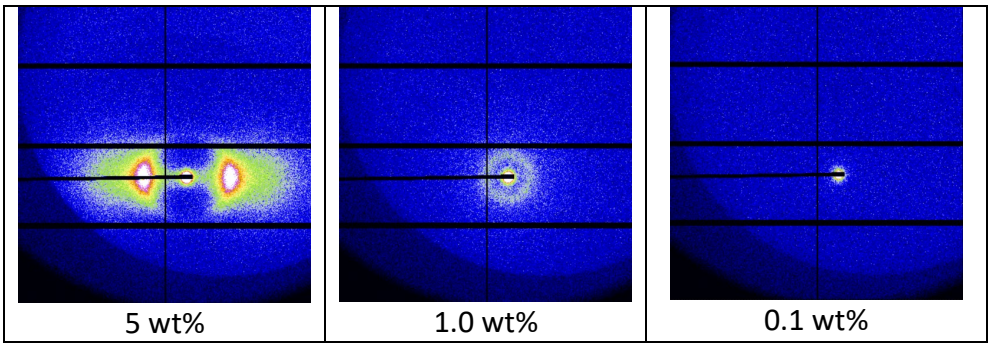

Figure 5.

The d-spacing obtained from the diffraction spots/rings is plotted for varying concentrations in Fig. 6. While theory predicts a scaling power law with an n = -0.5 exponent, our data point at a slightly different value, n = -0.43, which is probably indicative of clustering effects.

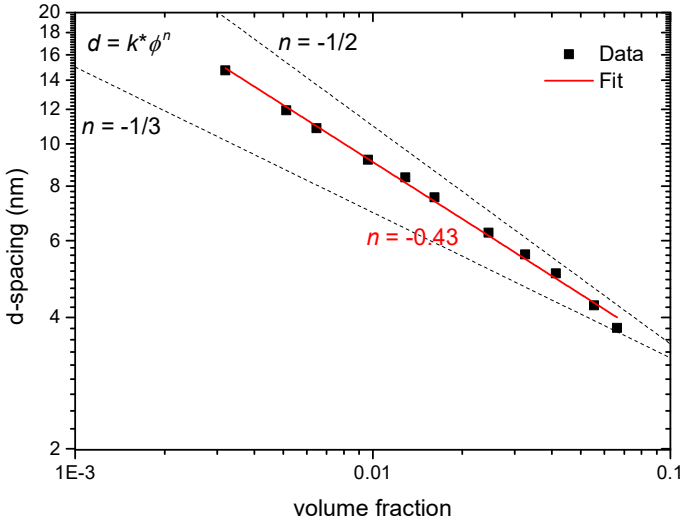

Figure 6.

The SAXS patterns taken on PBDT-GO solutions are a combination of the patterns discussed above, with the anisotropic GO scattering at low angle and the pair of PBDT diffraction spots at larger q values indicating the orthogonal alignemt of the GO and PBDT nematic directors ($\mathbf{n}_{GO}$ and $\mathbf{n}_{P}$, respectively), i.e. the formation of a biaxial N phase (see pattern and scheme of Fig. 7).

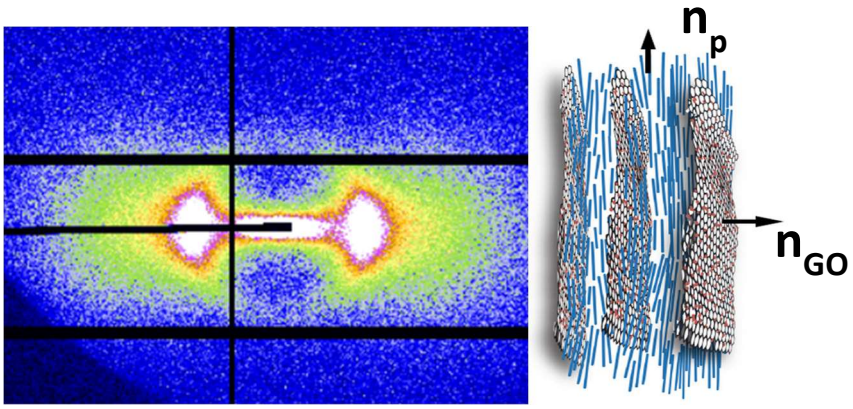

Figure 7.

Finally, the presence of GO seems to have little influence on the PBDT inter-rod distance, as evidence in Fig. 8, where the polymer *d*-spacings measured in neat PBDT solutions are compared to those omeasured in PBDT-GO solutions.

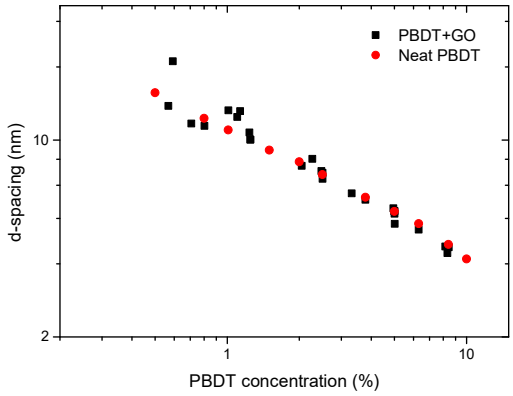

Figure 8.